Analysis using dielectric variation based hybrid-pol three-component model-based method

Ajeet Kumar†, *Student Member, IEEE,*, Anup Das‡, *Member, IEEE,*, and Rajib Kumar Panigrahi†, *Member, IEEE,*
† Department of ECE, IIT Roorkee, India; ‡ SAC, ISRO, India
email: ajeet.kumar.in@ieee.org

***Abstract*—In general, the full-polarimetry (full-pol) decomposition methods are established based on the scattering models with surface dielectrics, which is uncommon in the case of hybrid-polarimetry (hybrid-pol). The utilization of surface dielectric properties allows the decomposition methods to exhibit more realistic and clearer representation of the Earth's surface. This has been validated in case of hybrid-polarimetry by comparing the performance of HTM (a dielectric properties based method) with the previously reported $m-\delta$, $m-\alpha$, and modified $m-\chi$ methods. For comparative-evaluation, the original hybrid-pol data of RISAT-1 satellite, acquired over Mumbai city (India) is implemented.**

***Index Terms*—hybrid-pol, surface dielectrics, decomposition methods.**

I. Introduction

In past many years, full-polarimetry (full-pol or quad-pol) Synthetic Aperture Radar (SAR) systems have provided promising results for Earth surface monitoring. However, now-a-days, researchers are seeking alternative SAR configuration due to inherent demerits of full-pol based systems. The full-pol SAR based systems mainly suffers with the demerits related to less swath-coverage area, high transmitted-power (P_t) requirement, and constricted range of acceptance incidence-angle (θ_i). The reduced swath coverage of full-pol SAR system leads to adverse impact on revisit time, which is an important factor for the Earth observing community. Quad-pol SAR system transmits two pulses in one time slot, so it requires double transmission power than conventional single-pol SAR systems. Also, it receives orthogonal polarization for each one of the transmitted pulse which leads to four times increase in data rate in comparison with single-pol SAR. To overcome the drawbacks of full-pol SAR system and obtain the results closer to full-pol system, the compact-polarimetry (compact-pol) configuration is introduced in literature [1]. The compact-pol basically has three modes: $\pi/4$, dual circular-pol (DCP), and hybrid-polarimetry (hybrid-pol), among which hybrid-pol is established as an optimum one [2]. However for the analysis of hybrid-pol data, very few approaches are reported in the open literature. $m-\delta$ [2], $m-\alpha$ [3], $m-\chi$ [4], modified $m-\chi$ [5], and HTM [6] are four such methods which directly utilizes the Stokes vector information of hybrid-pol data for the analysis. In comparison with $m-\delta$, $m-\chi$ is more robust in the case when impure circular (due to significant existence of linearly polarized component in the transmitted field) based hybrid-pol data is used [4]. Moreover, $m-\chi$ obtains similar results as can be obtained by $m-\alpha$ [4], [7]. $m-\chi$ is further modified in [5] by utilizing "circular polarization ration (μ)", where μ improves the separation of single-bounce and double-bounce scattering mechanism. These, $m-\delta$, $m-\chi$, $m-\alpha$, and modified $m-\chi$ methods do not use "scattering models with surface dielectrics" [6]. Consequently, these methods are not able to provide realistic representation of the surface. Contrarily to this, the HTM, i.e. hybrid-pol three-component model-based decomposition method utilizes α and β which indicate co-polarization ratios for Bragg-surface scattering and dihedral-scattering, respectively. This α parameter is different than the α-angle used in $m-\alpha$. Co-polarization ratio parameters α and β depend on surface complex permittivity and local incidence angle [6], [8], [9]. HTM is further modified in [6] using μ to make more clear separation between single- and double-bounce scattering types.

II. $m-\delta$, $m-\alpha$, modified $m-\chi$, and modified HTM

Table I
Expressions of single-bounce (P_s), double-bounce (P_d), and volume scattering (P_v) contributions for different hybrid-pol methods using Stokes parameters/sub-parameters

Methods	Expressions
$m-\delta$	$\begin{bmatrix} P_s \\ P_d \\ P_v \end{bmatrix} = \begin{bmatrix} 0.5\times G_0\times m\times(1+\sin\delta) \\ 0.5\times G_0\times m\times(1-\sin\delta) \\ G_0\times(1-m) \end{bmatrix}$
$m-\alpha$	$\begin{bmatrix} P_s \\ P_d \\ P_v \end{bmatrix} = \begin{bmatrix} 0.5\times G_0\times m\times(1+\cos 2\alpha) \\ 0.5\times G_0\times m\times(1-\cos 2\alpha) \\ G_0\times(1-m) \end{bmatrix}$
Modified $m-\chi$	$\begin{bmatrix} P_s \\ P_d \\ P_v \end{bmatrix} = \begin{bmatrix} 0.5\times G_0\times m\times(1+\sin 2\chi) \\ {\mu_c}^2\times 0.5\times G_0\times m\times(1-\sin 2\chi) \\ G_0\times(1-m) \end{bmatrix}$
Modified HTM	$\begin{bmatrix} P_s \\ P_d \\ P_v \end{bmatrix}_{G_3>0} = \begin{bmatrix} \frac{({G_0'}^2+{G_1'}^2+{G_2'}^2+{G_3'}^2)+2G_0'\times G_3'}{2(G_0'+G_3')} \\ {\mu_c}^2\times\frac{({G_0'}^2-{G_1'}^2-{G_2'}^2-{G_3'}^2)}{2(G_0'+G_3')} \\ G_0-\sqrt{{G_1}^2+{G_2}^2+{G_3}^2} \end{bmatrix}$ $\begin{bmatrix} P_s \\ P_d \\ P_v \end{bmatrix}_{G_3<0} = \begin{bmatrix} \frac{({G_0'}^2-{G_1'}^2-{G_2'}^2-{G_3'}^2)}{2(G_0'-G_3')} \\ {\mu_c}^2\times\frac{({G_0'}^2+{G_1'}^2+{G_2'}^2+{G_3'}^2)-2G_0'\times G_3'}{2(G_0'-G_3')} \\ G_0-\sqrt{{G_1}^2+{G_2}^2+{G_3}^2} \end{bmatrix}$

The expressions of three basic scattering mechanisms using different hybrid-pol decomposition methods are shown in

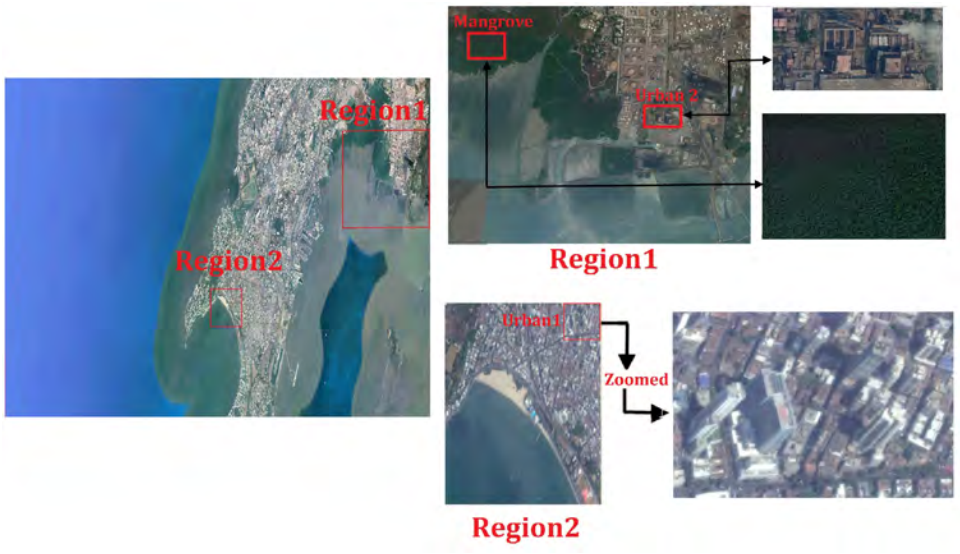

Figure 1. Google Earth optical description about the region under observation.

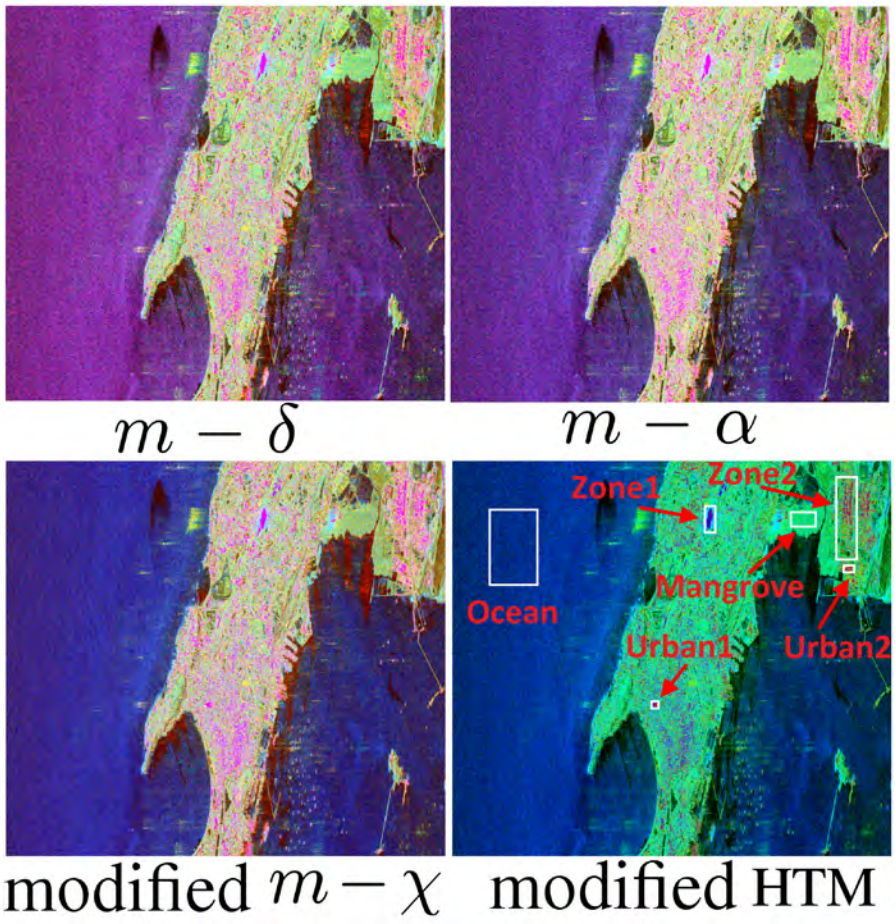

Figure 2. RGB Decomposition images of RISAT-1 Mumbai data using $m-\delta$, $m-\alpha$, modified $m-\chi$, and modified HTM .

Table I. The Stokes child or sub-parameters shown in Table I can be directly derived using Stokes vector [2], [3], [5], [10].

III. RISAT-1 DATA ANALYSIS DECOMPOSITION RESULTS

To evaluate the efficacy of dielectric variation based modified HTM method, various small regions: Ocean, Urban1,

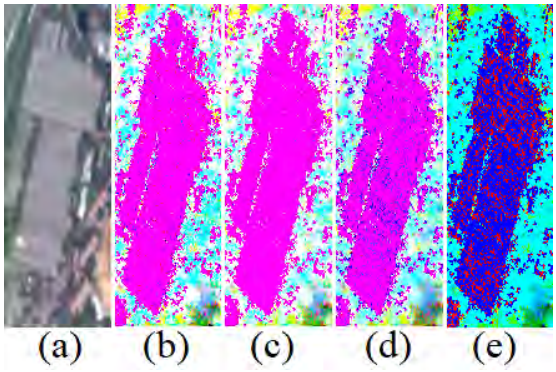

Figure 3. Zone1 image of (a) Google Earth (b) $m-\delta$, (c) $m-\alpha$, (d) modified $m-\chi$ and (e) modified HTM.

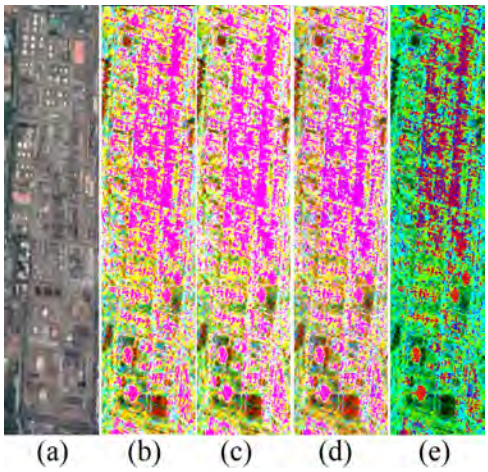

Figure 4. Zone2 images of (a) Google Earth (b) $m-\delta$, (c) $m-\alpha$, (d) modified $m-\chi$ and (e) modified HTM.

Urban2, Zone1, Zone2, Mangrove, are selected over RISAT-1 data of Mumbai region, as shown in Fig. 2. For ground truth visualization, the Google Earth optical image of the selected regions are shown in Fig. 1. One can clearly see that the selected urban regions include buildings and Mangrove region includes densely packed tree (mainly *Avincennia marina* tree species). The decomposed images of the selected area using $m-\delta$, $m-\alpha$, modified $m-\chi$, and modified HTM are shown in Fig. 2. By looking in these images, one can see that the RGB color composition for pixel indicating dominance of specific scattering mechanism is more clear in modified HTM decomposed image, in comparison with the decomposition images generated by $m-\delta$, $m-\alpha$, and modified $m-\chi$. For example, in the decomposition result obtained using modified HTM, the ocean, urban, and mangrove regions have clearer exhibition of blue, red and green colors, respectively, in comparison with $m-\delta$, $m-\alpha$, and modified $m-\chi$. This has been validated by selecting various small rectangular areas of different scattering types, indicated by white rectangles over Fig. 2. The selected "Zone 1" region contains shed covering Mumbai central railway station, which should have majority of surface-scattering (single-bounce) or blue pixels. On the other hand, "Zone 2" covers the region of Bharat-Petroleum-Refinery which contains urban buildings. These buildings generate dihedral-scattering mechanism, which should be indicated by red pixels. The visual results of "Zone 1" and "Zone 2" are shown in Fig. 3 & 4, respectively. Fig. 3(a), 3(b), 3(c), 3(d), and 3(e) indicate the enlarged version of "Zone 1" Google Earth image, $m-\delta$ decomposed image, $m-\alpha$ decomposed image, modified $m-\chi$ decomposed image, and modified HTM decomposed image, respectively. Similarly, Fig. 4(a), 4(b), 4(c), 4(d), and 4(e) indicate the enlarged version of "Zone 2" Google Earth image, $m-\delta$ decomposed image, $m-\alpha$ decomposed image, modified $m-\chi$ decompose image, and modified HTM decomposed image, respectively. By looking in these images, following observations can be made.

- The decomposed RGB images of "Zone 1" containing railway-station's shed (mostly covers surface-scattering type pixels) and "Zone 2" containing double-bounce scattering type buildings, have majority of pixels with same color (pink) in the decomposed result of $m-\delta$, $m-\alpha$, and modified $m-\chi$.
- On the other hand, the railway-station's shed in "Zone1" and buildings in "Zone 2" mostly consists of blue and red color pixels, respectively, in the decomposed RGB images obtained using modified HTM technique.

Also, by looking in all four decomposition results shown in Fig. 2, one can observe that the mangrove or vegetation region is clear green in modified HTM method, whereas reddishness can be seen in the results obtained using other decomposition methods. The reason of this reddishness is analyzed. We have plotted the contribution of double-bounce power contribution, i.e. P_d, along with the dominating volume scattering contribution, i.e. P_v, for the selected Mangrove region. The corresponding plots are shown in Fig. 5. By analyzing the plots shown in Fig. 5(a), 5(d), 5(e), and 5(h), which corresponds to the mangrove results obtained using $m-\delta$, $m-\alpha$, modified $m-\chi$, and modified HTM, respectively, following observations can be made.

- The decomposition images of mangrove region, as shown in 5(b), 5(c), and 5(f), obtained using $m-\delta$, $m-\alpha$, and modified $m-\chi$, respectively, contain yellowish and reddish pixels along with the green. Whereas, the HTM decomposed image of mangrove region, as shown in 5(g), contains mostly green pixels. The reason of this is explained using P_d and P_v plots in the next point.
- For the mangrove region pixels, the undesirable double-bounce contribution can be clearly observed in the case of $m-\delta$, $m-\alpha$, and modified $m-\chi$. Contrarily, the double-bounce contribution, i.e. P_d is much lesser than P_v in the case of HTM. Due to this reason, the reddishness is not there in the mangrove decomposition result obtained using HTM. Consequently, the clearer interpretation of dominant scattering type can be seen in HTM decomposition result.

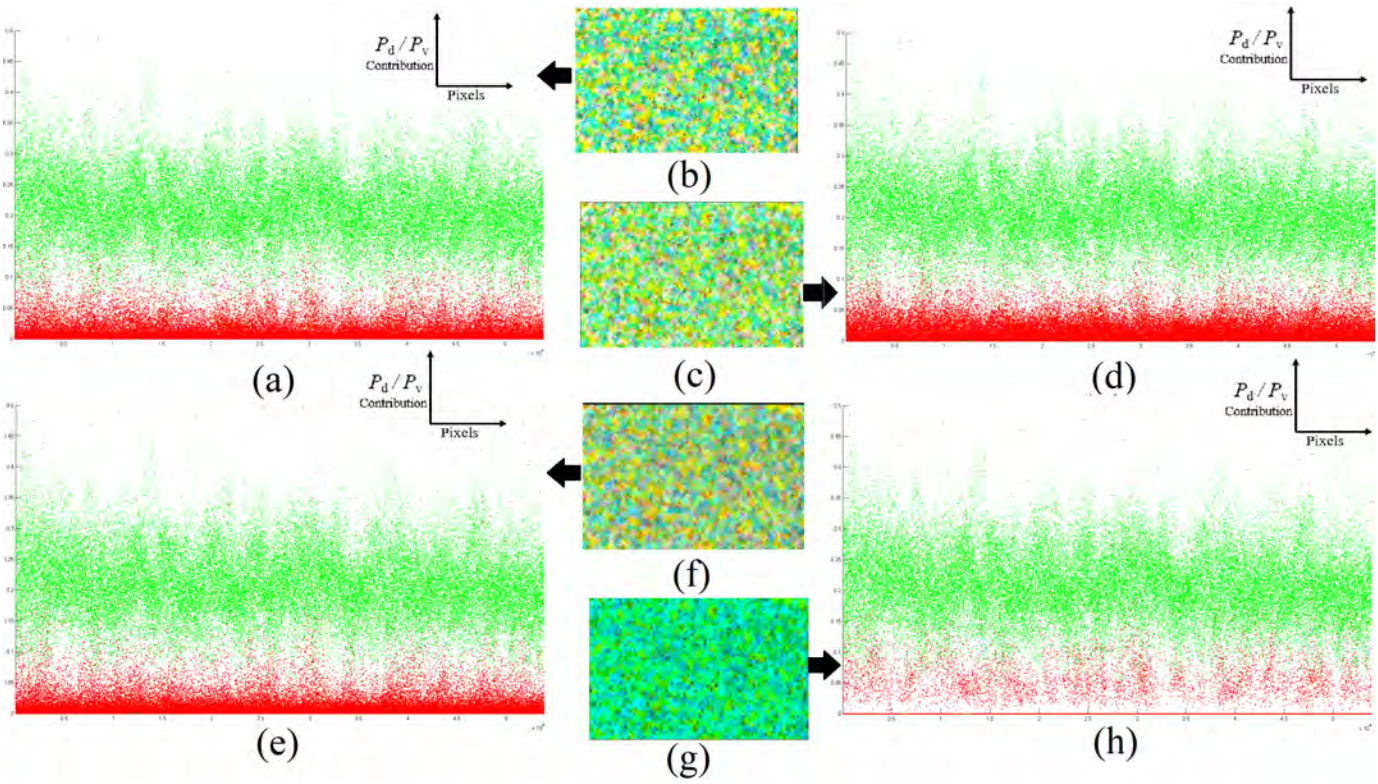

Figure 5. Mangrove region results: (a) P_d & P_v contribution plot of Mangrove region using $m-\delta$ (b) RGB decomposed result of Mangrove region using $m-\delta$ (c) RGB decomposed result of mangrove region using $m-\alpha$ (d) P_d & P_v contribution plot of Mangrove region using $m-\alpha$ (e) P_d & P_v contribution plot of Mangrove region using modified $m-\chi$ (f) RGB decomposed result of Mangrove region using modified $m-\chi$ (g) RGB decomposed result of mangrove region using HTM (h) P_d & P_v contribution plot of Mangrove region using HTM.

IV. Conclusion

In the case of dielectric-variation based hybrid-pol decomposition method, i.e. HTM, the dominant scattering types of single-bounce, double-bounce, and volume scattering mechanisms are more clearly exhibited by blue, red, and green colors, respectively. The reason behind better decomposition results has been explained by plotting the power contribution values of dominant as well as non-dominant scattering mechanisms. As shown in the results, the contribution of non-dominating scattering mechanisms is very less in HTM, in comparison with other reported methods, such as $m-\delta$, $m-\alpha$, and modified $m-\chi$. It shows that the utilization of surface dielectric variations in hybrid-pol decomposition methods provide more clear and realistic representation of Earth's surface.

Acknowledgment

Part of the work presented in this paper is funded by ISRO under the RESPOND project via sanction number ISRO/RES/4/609/2013-14.

References

[1] J.-C. Souyris, P. Imbo, R. Fjortoft, S. Mingot, and J.-S. Lee, "Compact polarimetry based on symmetry properties of geophysical media: The $\pi/4$ mode," *IEEE Transaction on Geoscience and Remote Sensing*, vol. 43, no. 3, pp. 634–646, Mar. 2005.

[2] R. K. Raney, "Hybrid-polarity SAR architecture," *IEEE Transaction on Geoscience and Remote Sensing*, vol. 45, no. 11, pp. 3397–3404, Nov. 2007.

[3] S. R. Cloude, D. G. Goodenough, and H. Chen, "Compact decomposition theory," *IEEE Geoscience and Remote Sensing Letter*, vol. 9, no. 1, pp. 28–32, Jan. 2012.

[4] R. K. Raney, J. T. S. Cahill, G. W. Patterson, and D. B. J. Bussey, "The $m-\chi$ decomposition of hybrid dual-polarimetric radar data," *Geoscience and Remote Sensing Symposium (IGARSS)*, pp. 5093–5096, Jul. 2012.

[5] R. Sabry and P. W. Vachon, "A unified framework for general compact and quad polarimetric SAR data and imagery analysis," *IEEE Transactions on Geoscience and Remote Sensing*, vol. 52, no. 1, pp. 582–602, Jan. 2014.

[6] A. Kumar, A. Das, and R. K. Panigrahi, "Hybrid-pol based three-component scattering model for analysis of RISAT data," *IEEE Journal of Selected Topics in Applied Earth Observations and Remote Sensing*, vol. 10, no. 12, pp. 5155–5162, Dec. 2017.

[7] G. G. Ponnurangam, T. Jagdhuber, I. Hajnsek, and Y. S. Rao, "Soil moisture estimation using hybrid polarimetric SAR data of RISAT-1," *IEEE Transactions on Geoscience and Remote Sensing*, vol. 54, no. 4, pp. 2033–2049, Apr. 2016.

[8] A. Freeman and S. L. Durden, "A three-component scattering model for polarimetric SAR data," *IEEE Transaction on Geoscience and Remote Sensing*, vol. 36, no. 3, pp. 963–973, May 1998.

[9] J. sen Lee and E. Pottier, *Polarimetric radar imaging: From basics to applications*. Boca Raton, US: CRC Press, Taylor and Francis group, 2009.

[10] A. Kumar, A. Das, and R. K. Panigrahi, "Hybrid-pol decomposition methods: A comparative evaluation and a new entropy-based approach," *IETE Technical Review*, vol. 37, no. 3, pp. 296–308, 2020.